The Role of Interstitial Sites in the Ti*3d* Defect State in the Band Gap of Titania

Stefan Wendt,[1] Phillip T. Sprunger,[1,2] Estephania Lira,[1] Georg K. H. Madsen,[1] Zheshen Li,[1] Jonas Ø. Hansen,[1] Jesper Matthiesen,[1] Asger Blekinge-Rasmussen,[1] Erik Lægsgaard,[1] Bjørk Hammer,[1]* Flemming Besenbacher[1]*

Titanium dioxide (TiO_2) has a number of uses in catalysis, photochemistry, and sensing that are linked to the reducibility of the oxide. Usually, bridging oxygen (O_{br}) vacancies are assumed to cause the Ti*3d* defect state in the band gap of rutile TiO_2(110). From high-resolution scanning tunneling microscopy and photoelectron spectroscopy measurements, we propose that Ti interstitials in the near-surface region may be largely responsible for the defect state in the band gap. We argue that these donor-specific sites play a key role in and may dictate the ensuing surface chemistry, such as providing the electronic charge required for O_2 adsorption and dissociation. Specifically, we identified a second O_2 dissociation channel that occurs within the Ti troughs in addition to the O_2 dissociation channel in O_{br} vacancies. Comprehensive density functional theory calculations support these experimental observations.

Titanium dioxide (TiO_2), or titania, is used in a number of technological areas, including heterogeneous catalysis, photocatalysis, solar cells, gas sensors, waste remediation, and biocompatible materials. In its stoichiometric form, titania is an inert wide–band gap insulator; however, its applications are enabled by excess electrons originating from the defect state that is located within the band gap of reduced titania (TiO_{2-x}). Understanding the origin of the defect state is important for improving or expanding the scope of titania-based systems for specific applications. For example, the enhanced catalytic activity of titania-supported gold nanoparticles is coupled to local properties at the interface between gold and reduced titania (*1*–*4*).

Conventionally, the Ti*3d* derived state in the band gap (*5*–*7*) at ~0.85 eV below the Fermi level (E_F) has been fully ascribed to bridging oxygen (O_{br}) vacancies, because, in an ionic picture, the two excess electrons per O_{br} vacancy may be transferred to neighboring Ti atoms (*5*, *6*, *8*–*11*). This hypothesis was proposed more than three decades ago based on ultraviolet photoelectron spectroscopy (UPS) and low-energy electron-diffraction measurements on the TiO_2(110)–(1 × 1) surface (*8*), and has been generally accepted for years (*5*, *6*, *9*, *11*). In the UPS studies, this proposed O-vacancy model has largely been based on experimental observations that the defect state can be eliminated by O_2 exposure (*8*, *12*, *13*). Further possible support for the O-vacancy model came from scanning tunneling microscopy (STM) (*14*–*17*) and atomic force microscopy (*18*) studies, where O_{br} vacancies have been clearly identified on TiO_2(110). Although most first-principles density functional theory (DFT) calculations have not reproduced the experimentally observed state in the band gap (*11*), numerous theoretical papers still favor the O-vacancy model (*6*, *11*).

Nevertheless, the importance of Ti interstitials in rutile TiO_2(110) crystals has been noted. For example, the reoxidation of sputtered TiO_2(110) surfaces via vacuum annealing has been explained by Ti interstitial diffusion into the bulk (*19*–*21*). Similarly, when a reduced TiO_2(110) crystal is exposed to O_2 at elevated temperatures, diffusion of Ti interstitials to the surface has been reported (*2*, *22*–*24*). Therefore, in addition to O vacancies, Ti interstitials must also be considered as defect sites that may influence and even dictate the surface chemistry of titania.

By means of high-resolution STM and photoelectron spectroscopy (PES) measurements in conjunction with DFT calculations, we have systematically explored the origin of the Ti*3d* defect state in the band gap. We found that the gap state remains almost unchanged on surfaces where the O_{br} vacancies (or bridging OH groups) have been removed. To explain this finding, we propose that the gap state mainly stems from surplus Ti atoms in the near-surface region, most likely on interstitial sites. In addition to an O_2 dissociation channel in O_{br} vacancies, we discovered a non–vacancy-related O_2 dissociation channel that occurs within the Ti troughs.

The TiO_2(110)–(1 × 1) surface consists of alternating rows of fivefold-coordinated Ti (5f-Ti) atoms (the Ti troughs) and protruding, twofold-coordinated O_{br} atoms. As bulk Ti atoms in stoichiometric rutile, the Ti atoms underneath the O_{br} atoms are sixfold-coordinated. Ion-sputtering and vacuum-annealing the TiO_2(110) crystal results in a reduced n-type semiconductor, with a bulk conductivity that allows the use of STM and other electron spectroscopy techniques. Consistent with previous findings (*6*), the STM images (Fig. 1) of the TiO_2(110) surface are dominated by electronic effects; that is, the bright rows correspond to the Ti troughs, whereas geometrically protruding O_{br} atoms appear as the dark troughs in the STM images (*6*).

A high-resolution STM image recorded on a clean reduced TiO_2(110) surface [*r*-TiO_2(110)]

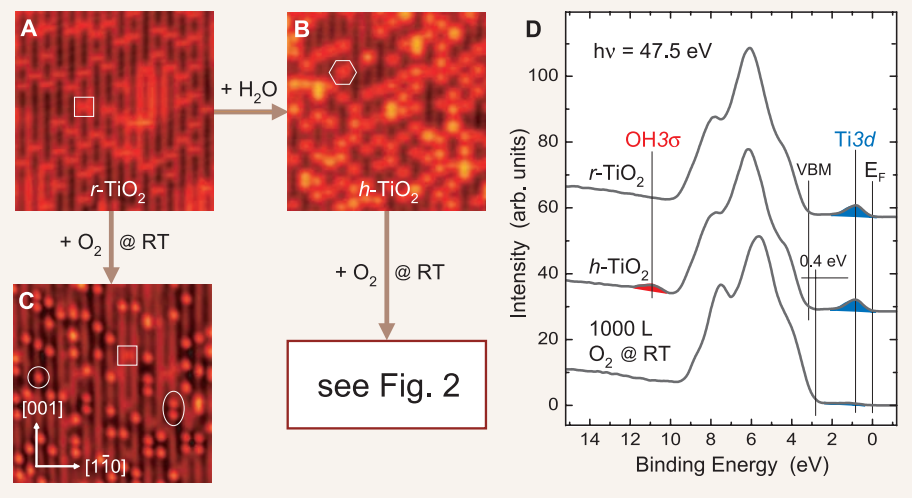

Fig. 1. STM images (105 by 105 Å) of *r*-TiO_2(110) (**A**), *h*-TiO_2(110) (**B**), and a RT O_2-saturated TiO_2(110) surface (**C**) acquired using a sample in a reduction state corresponding to an O_{br}-vacancy density of 11.4 ± 0.3% MLs. Symbols indicate O_{br} vacancies (square), capping H atoms (hexagon) in the O_{br} rows, and O_{ot} adatoms (circle), as well as pairs of next-nearest O_{ot} adatoms (ellipse) in the Ti troughs. STM images were collected with a tunneling current (I_t) ≤ 0.1 nA and a tunneling voltage (V_t) = 1.2 V. Directions throughout the paper are identical to those indicated in (C). Corresponding PES valence-band spectra are shown in (**D**). PES spectra and STM images were recorded at sample temperatures between 100 and 130 K. The position of the valence-band maximum is indicated by VBM and the Ti*3d* defect state is observed within the ~3.1-eV-wide band gap.

[1]Interdisciplinary Nanoscience Center (iNANO), Department of Physics and Astronomy, and Institute for Storage Ring Facilities, University of Aarhus, DK-8000 Aarhus C, Denmark. [2]Department of Physics and Astronomy, Louisiana State University, Baton Rouge, LA 70808, USA.

*To whom correspondence should be addressed. E-mail: hammer@phys.au.dk (B.H.); fbe@inano.dk (F.B.)

(Fig. 1A) shows faint protrusions that appear between the bright Ti troughs and that correspond to O_{br} vacancies in the O_{br} rows (*14*–*17*). Starting from an *r*-TiO_2(110) surface, we studied the effect of hydration by letting water dissociate in the O_{br} vacancies (Fig. 1B). The brighter protrusions in the O_{br} rows appearing on the resulting hydrated TiO_2(110) surface [*h*-TiO_2(110)] originate from capping H atoms or, in an alternative notation, from OH_{br} groups (*14*–*17*). In the PES valence-band spectra corresponding to *r*- and *h*-TiO_2(110) (Fig. 1D), the only obvious difference is the OH3σ feature at a binding energy (BE) of ~10.8 eV that is evident in the valence band after hydration (*12*). The Ti*3d* defect state at ~0.85 eV below E_F is only minimally affected by hydration, in spite of the complete absence of O_{br} vacancies on *h*-TiO_2(110).

In an attempt to "heal" the O_{br} vacancies on *r*-TiO_2(110) without producing capping H atoms on the O_{br} rows, we studied the interaction of O_2 with clean *r*-TiO_2(110) at room temperature (RT). The number of O_{br} vacancies decreased after the O_2 exposure (Fig. 1C), and a number of bright spots appeared simultaneously on the Ti troughs, some of which are next-nearest neighbors. Based on previous O_2 interaction experiments (*3*, *14*, *25*), the spots in the Ti troughs are assigned to O adatoms that reside on top of 5f-Ti atoms (O_{ot}). However, O_2 exposure at RT does not lead to the healing of all the O_{br} vacancies, even in the case of saturation (*26*). In the valence-band spectrum corresponding to the O_2-exposed TiO_2(110) surface, one feature is the strongly suppressed defect state at ~0.85 eV (Fig. 1D). In addition, compared with the spectra for *r*- and *h*-TiO_2(110), the dominating features between BEs of ~3 and ~9.5 eV [primarily O2*p*-derived (*5*, *7*, *12*, *27*)] were found to be shifted by ~0.4 eV toward E_F.

Both of these adsorption experiments, hydration of *r*-TiO_2(110) as well as oxidation of *r*-TiO_2(110) at RT, raise questions about the origin of the Ti*3d* defect state. In the case of the *h*-TiO_2(110) surface, the assignment of the defect state is hampered because of capping H atoms, which also could lead to a state in the band gap (*10*). Because O_2 exposure at RT to *r*-TiO_2(110) leads to a surface with O_{ot} adatoms and residual O_{br} vacancies, and not to a TiO_2(110) surface that is characterized by perfect O_{br} rows as was previously assumed (*8*), this experiment also does not reveal the origin of the defect state. In order to assign the Ti*3d* defect state, TiO_2(110) surfaces need to be prepared that are characterized by perfect O_{br} rows without O_{br} vacancies and capping H atoms, and by Ti troughs without O_{ot} adatoms.

Motivated by the observation that the capping H atoms on the O_{br} rows can be reacted off via reaction with O_2 (*28*), we exposed *h*-TiO_2(110) surfaces to O_2 at RT (Fig. 2). As revealed by the STM images depicted in Fig. 2, A to D, it is possible to react off all capping H atoms from the O_{br} rows and create a TiO_2(110) surface with perfect O_{br} rows. However, for O_2 exposures greater than an optimum value, all of the capping H atoms were removed, but additionally, new surface species with an elongated shape appeared within the Ti troughs (Fig. 2, C and D).

We considered the PES results acquired with surface preparations identical to those in the STM experiments and focused on the OH3σ feature at ~10.8 eV and on the Ti*3d* defect state (Fig. 2E). The OH3σ feature was completely attenuated after an O_2 exposure of 4 Langmuirs (L 1L = 1.33 × 10^{-6} mbar·sec, whereas much higher exposures were required to minimize the Ti*3d* defect state (420 L). For clarity, the evolutions of the Ti*3d* defect state and the OH3σ feature are shown in Fig. 2F in greater detail, and the development of the OH3σ feature for O_2 exposures of ≤4 L is shown in fig. S1 (*26*). One observation from Fig. 2F is that for 4-L O_2 exposure, where the TiO_2(110) surface is characterized by perfect O_{br} rows and essentially without capping H atoms, the Ti*3d* defect state was only slightly attenuated. In complete contradiction to the conventionally accepted O-vacancy model, the PES valence spectra in Fig. 2 reveal that the Ti*3d* defect state

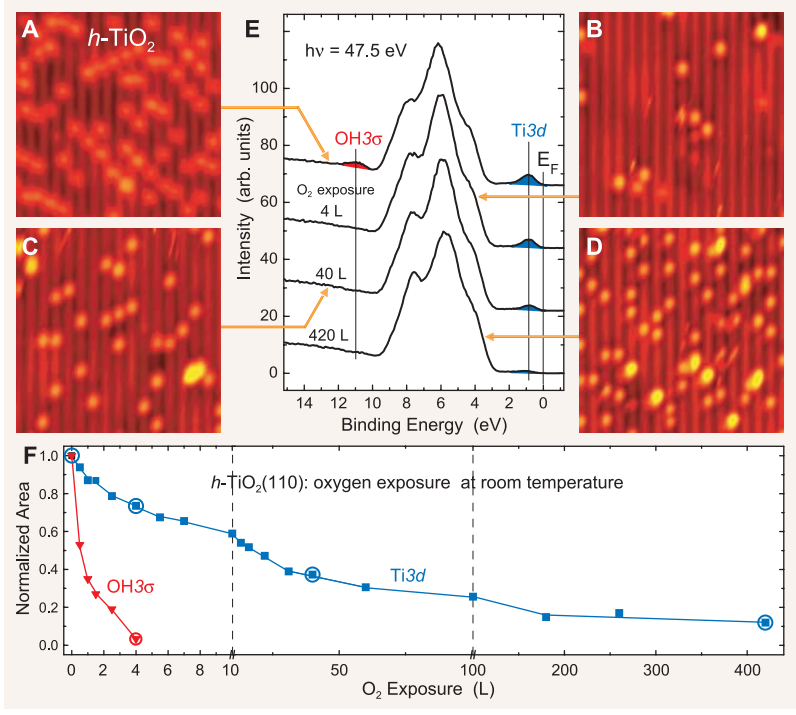

Fig. 2. (**A** to **D**) STM images (105 by 105 Å) of an *h*-TiO_2(110) surface that was exposed to increasing amounts of O_2 at RT. For these experiments we used a TiO_2(110) crystal with an O_{br}-vacancy density of 5.5 ± 0.2% MLs. (**E**) Selected PES valence-band spectra recorded on an *h*-TiO_2(110) surface that was exposed to O_2 at RT. Arrows indicate the representative STM images. For the PES experiments, a TiO_2(110) crystal was used with an O_{br}-vacancy density of 11.4 ± 0.3% MLs. (**F**) Normalized integrated intensities of the OH3σ (red) and Ti*3d* (blue) features for O_2 exposures up to 420 L from PES spectra; circles indicate intensity values that were obtained from the spectra shown in (E).

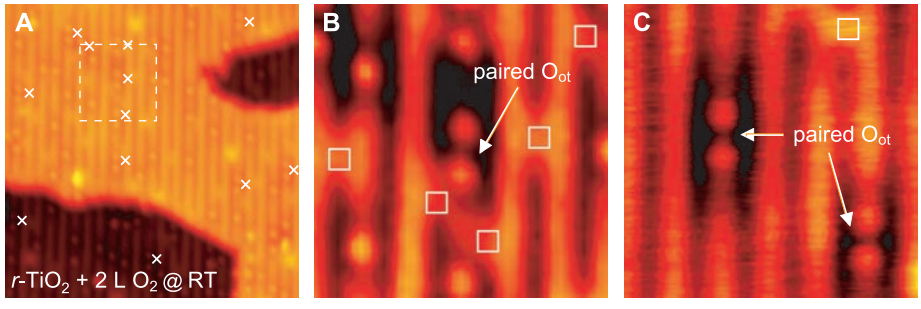

Fig. 3. STM results illustrating the reaction of O_2 with *r*-TiO_2(110) at RT. (**A**) STM image (155 by 155 Å) acquired after 2-L O_2 exposure. White crosses indicate pairs of next-nearest O_{ot} adatoms. (**B**) Zoom-in STM image (38 by 38 Å) of the area indicated by the dashed white square in (A). White squares indicate O_{br} vacancies. (**C**) Zoom-in STM image (38 by 38 Å) acquired after 200-L O_2 exposure at RT. Before the O_2 exposure, this *r*-TiO_2(110) crystal was characterized by an O_{br}-vacancy density of only ~1.7% MLs. STM images were acquired at temperatures between 110 and 130 K.

is caused by neither O_{br} vacancies nor capping H atoms on the O_{br} rows. Rather, we will show in the following that the Ti*3d* defect state can be directly correlated with the existence of near-surface Ti interstitial defect sites. Within this model, electronegative adsorbates, such as those shown in Fig. 2, C and D, are stabilized on TiO_2(110) surfaces with perfect O_{br} rows through charge transfer from Ti interstitials to the adsorbates.

Given the possibility of electron donation arising from Ti interstitial defects, we studied the interaction of O_2 with the clean *r*-TiO_2(110) surface at RT in further detail (Fig. 3). Specifically, we identified a non–vacancy-related O_2 dissociation channel occurring within the Ti troughs. That such a second O_2 dissociation channel exists, in addition to the known dissociation channel associated with O_{br} vacancies (*3*, *14*, *16*, *29*, *30*), is evident from the high number of paired O_{ot} adatoms observed on a partially oxidized *r*-TiO_2(110) surface (Fig. 3, A and B). After O_2 exposure, the densities of O_{br} vacancies {3.9% monolayers [MLs; 1 ML is the density of the (1 × 1) units, 5.2×10^{14} cm^{-2}]} and O_{ot} adatoms (6.0% MLs) together exceed the density of O_{br} vacancies before the exposure (7.9% MLs) by roughly the density of O_{ot} adatoms found in pairs (1.7% MLs). In the pairs, two O_{ot} adatoms are adsorbed on next-nearest Ti-5f atoms. Such O_{ot} pairs were also observed after oxidation of an *r*-TiO_2(110) surface with a very low density of O_{br} vacancies (Fig. 3C), where an unlikely but, in principle, possible O_{ot} pair formation through two separate O_2 dissociation reactions in O_{br} vacancies on adjacent O_{br} rows can be ruled out with certainty. O_{ot} pairs are also evident in the STM images reported by Henderson *et al.* (*25*).

To study the non–vacancy-related O_2 dissociation channel more in depth, we also exposed *r*-TiO_2(110) surfaces to O_2 at low temperatures (120 K) and subsequently annealed the crystals to temperatures of 393 K and 448 K, respectively (Fig. 4, A to E). After exposing the surface of a TiO_2(110) crystal with an O_{br} vacancy density of 4.5% MLs to 5 L of O_2 at 120 K, all the O_{br} vacancies disappeared and O_{ot} adatoms appeared in the Ti troughs (Fig. 4A). No O_{ot} pairs were evident in the STM images, indicating that the non–vacancy-related O_2 dissociation channel does not operate at this low temperature. This conclusion is consistent with the 1:1 correlation between the density of O_{br} vacancies before O_2 exposure and the density of O_{ot} adatoms after the exposure. However, after annealing this O_2-exposed TiO_2(110) surface to 393 K (Fig. 4B), the density of O_{ot} adatoms increased by a factor of ~2. This result shows that the non–vacancy-related O_2 dissociation channel is energetically more activated than the one associated with the O_{br} vacancies.

In addition, a number of small islands appeared on the terraces, one of which is indicated in Fig. 4B by a circle. These newly formed islands are positioned in between two Ti troughs and show up in the STM images with a height of ~2.2 Å. Subsequent annealing to an even higher temperature (448 K) led to an increase in the density of the islands, and, in this case, larger islands with a height of ~3.2 Å were observed, in addition to the small islands (Fig. 4C). A height of ~3.2 Å closely resembles the step height on TiO_2(110) crystals; that is, the height of one TiO_2 trilayer, which is ~3.25 Å. When applying identical experimental procedures for a more reduced TiO_2(110) crystal (with an O_{br} vacancy density of ~10.8% MLs and ~9.4% MLs O_{ot} adatoms density after saturation with 20 L O_2 at 120 K), the density of O_{ot} adatoms was slightly smaller after annealing to 393 K than before the anneal (Fig. 4, D and E), but, compared with the situation on the low-reduced TiO_2(110) crystal (Fig. 4B), the number of small islands after annealing to 393 K was higher.

In Fig. 4F, we present PES results for a similar annealing experiment. The Ti*3d* defect state reappeared after annealing to temperatures higher than 400 K. In Fig. 4F, the oxidation before the annealing at 400 K was carried out at RT, but we found results when the oxidation was performed at 120 K that were similar to those of the STM experiments depicted in Figs. 4, A to E. Concomitant with the recovery of the Ti*3d* defect state, the valence-band maximum (VBM) shifts back to the original value of the clean *r*-TiO_2(110) surface.

Based on the STM results (Fig. 4, A to E) and the PES data (Fig. 4F and figs. S2 and S3) (*26*), we propose the following model. Because exclusively Ti and O features are evident in the PES core-level spectra (fig. S2), the islands appearing on previously flat terraces must be newly formed TiO_x structures, with x ~ 2. This finding implies that Ti atoms have diffused from the near-surface region to the topmost surface layer, where reactions with O_{ot} adatoms and possibly also

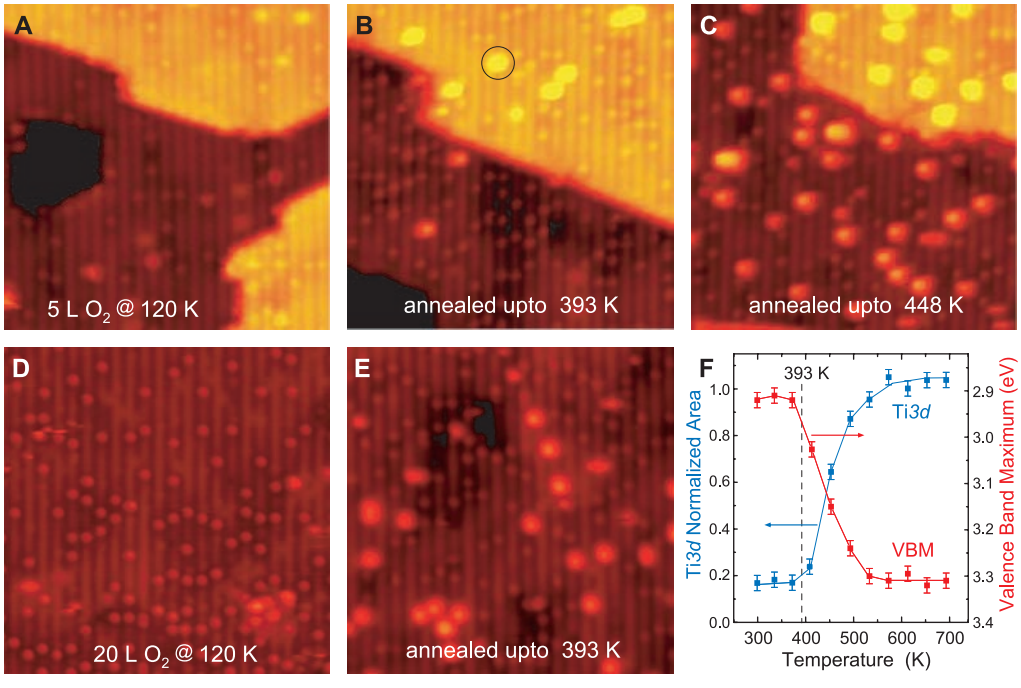

Fig. 4. (**A** to **C**) STM images (150 by 150 Å) of a TiO_2(110) crystal characterized by an O_{br}-vacancy density of ~4.5% MLs, (A) exposed to 5-L O_2 at 120 K, (B) subsequently annealed up to 393 K, and (C) further annealed up to 448 K. The circle in (B) indicates one of the newly formed TiO_x islands on the terraces with an STM height of ~2.2 Å. (**D** and **E**) STM images (150 by 150 Å) of a TiO_2(110) crystal characterized by an O_{br}-vacancy density of ~10.8% MLs, (D) exposed to 20-L O_2 at 120 K leading to an O_{ot} adatoms density of ~9.3% MLs and ~1.8% MLs residual O_{br} vacancies, and (E) after subsequent annealing up to 393 K where TiO_x islands have been formed. All STM images were acquired at temperatures between 110 and 130 K. Corresponding PES core-level scans are plotted in fig. S2 (*26*). Exclusively Ti- and O-related features were found in the PES spectra both after O_2 exposure at 120 K as well as after annealing to temperatures of ≥400 K. (**F**) Normalized integrated intensities of the Ti*3d* features (left axis, blue) and position of the VBM (right axis, red) as a function of the maximum annealing temperature. The VBM values are given in BE. The underlying valence-band spectra (fig. S3) were of an *r*-TiO_2(110) crystal that was reduced comparably to those crystals that were used to collect the data shown in Fig. 1 and Fig. 4, D and E. The crystal was oxidized at RT by exposing it to 1000 L of O_2.

with O_2 molecules occurred. The fact that the Ti*3d* defect state reappears after annealing to temperatures higher than 400 K can be explained by the migration of Ti interstitials from deeper layers to interstitial sites in the layers nearer the surface that had been depleted in the course of TiO_x island formation. Assuming a 1:2 correlation between Ti and O in the islands, we estimated a lower limit of Ti interstitials in the near-surface region, corresponding to 5 to 6% MLs for the TiO_2(110) crystals used in the experiments summarized in Fig. 4.

The STM and PES results shown in Fig. 4 are consistent with the temperature-programmed static secondary ion mass spectrometry data reported by Henderson (*19*), in which the onset of Ti interstitial diffusion occurred at ~400 K. Furthermore, similarities exist to previous STM results by Onishi *et al.* (*22*) and by Li *et al.* (*23*), in which O_2-induced growth of new structures on originally flat TiO_2(110) terraces were also obtained. However, because the experimental procedures applied in these previous studies were different from the ones in the present work, the structures obtained by Onishi *et al.* (*22*) and by Li *et al.* (*23*) are different from the ones obtained here.

The above-presented results addressing the O_2 interaction with *r*-TiO_2(110) reveal that Ti charge donors exist in the near-surface region of vacuum-annealed TiO_2 crystals, and that these donor sites strongly influence the O_2 interaction with *r*-TiO_2(110), even at temperatures as low as 120 K. Because the gap state remains largely unaffected by the removal of all surface defects (O_{br} and OH_{br}), we propose that the appearance of the gap state on clean reduced TiO_2(110) crystals, as is typically observed after vacuum annealing, is mainly associated with the Ti interstitials. Quenching of the gap state and so-called band-bending effects (Figs. 1D and 4F) can be ascribed to the withdrawal of electronic charge from the donor sites in the near-surface region through the accumulation of electronegative adsorbates, such as O_2 and O_{ot} adatoms on the surface.

To further explore this new interpretation, we performed first-principles DFT calculations using the DACAPO software package (https://wiki.fysik.dtu.dk/dacapo), using ultrasoft pseudopotentials and the revised Perdew-Burke-Ernzerhof exchange-correlation functional (*26*). We assumed a Ti interstitial (Fig. 5, blue) initially between the second and third trilayers of a five-TiO_2 trilayer slab with a $c(4 \times 2)$ surface-unit cell (Fig. 5B). On the surface of such a slab, an adsorbed O_2 molecule binds with ~1.6 eV, which is comparable to the ~1.9- and 0.8-to-2.0-eV bond strengths calculated for O_2 on *r*-TiO_2(110) (*14*) and *h*-TiO_2(110) (*31*), respectively. The DFT potential-energy diagram (Fig. 5A) shows that an energetically favorable pathway exists for a Ti interstitial to diffuse to the surface and to react with the adsorbed O_2 molecule to form a TiO_2 island on the terrace. The Ti interstitial diffusion proceeds via an exchange mechanism (*21*), in which a Ti atom on a regular lattice site (light blue) is released to an interstitial site toward the surface (Fig. 5C), and subsequently the lattice site is occupied by the original Ti interstitial atom (dark blue) from a deeper layer (Fig. 5D). Dissociation of the O_2 molecule (Fig. 5, E and F) gains ~4 eV in energy.

Relative to the initial configuration (Fig. 5B), the overall barrier for the formation of the TiO_x islands on the terraces is ~0.75 eV. However, with respect to the potential energy of the metastable intermediate configuration of the Ti interstitial between the first and second TiO_2 trilayer (Fig. 5C), the barrier becomes ~1.2 eV. The absolute value of this energy barrier is in good agreement with the experimental findings that the TiO_x islands appear on the flat TiO_2(110) terraces after annealing to temperatures well above RT (Fig. 4). If we tentatively assume that the Ti diffusion can be described as a first-order process, our rough estimate of the diffusion barrier from the Redhead formula is 1.2 eV.

If we start with a configuration wherein the O_2 molecule in Fig. 5 is replaced by an O_{ot} adatom, our DFT calculations still indicate favorable energetics for the diffusion of the Ti interstitial toward the surface. The two adsorbates, O_2 and O_{ot} adatoms, are quite similar electronically. According to a Bader charge analysis of our slab systems (*26*), a molecularly adsorbed O_2 species withdraws ~0.9 electron (*e*) from the TiO_2(110) substrate, whereas an O_{ot} adatom withdraws ~0.8 *e*. If these electronegative adsorbates are removed from the TiO_2(110) surface layer, the most favorable position of the Ti interstitial is the octahedral site (*32*) between the second and third TiO_2 trilayer. For a six-TiO_2 trilayer slab, our calculations show that the potential energy is higher by ~0.40 and ~0.23 eV, respectively, when locating the Ti interstitial one-TiO_2 trilayer higher or lower in the [110] direction.

To elucidate the mechanism of the second O_2 dissociation channel identified experimentally in Fig. 3 and Fig. 4, A and B, we performed additional calculations (figs. S4 and S5) (*26*). In agreement with previous reports (*14*, *33*, *34*), we found that O_2 molecules neither adsorb nor dissociate on stoichiometric TiO_2(110) unless the slab is reduced. Introduction of an O_{br} vacancy is sufficient to enable the adsorption of molecular O_2 (fig. S4B) (*26*) but not to dissociate O_2 in the Ti trough (fig. S4C) (*26*). Instead, when reducing the slab by adding a near-surface Ti interstitial, both the molecular (fig. S4D) and the dissociative adsorption (fig. S4E) of O_2 become feasible. If a Ti interstitial and an O_{br} vacancy occur simultaneously, the energy gain is even greater in both these adsorption modes (fig. S4, F and G). The experimental observation in Fig. 3 and Fig. 4, A and B, that dissociation of O_2 in the Ti troughs leads to next-nearest neighbors of O_{ot} adatoms is supported by the calculated preference for this configuration (fig. S5D) as com-

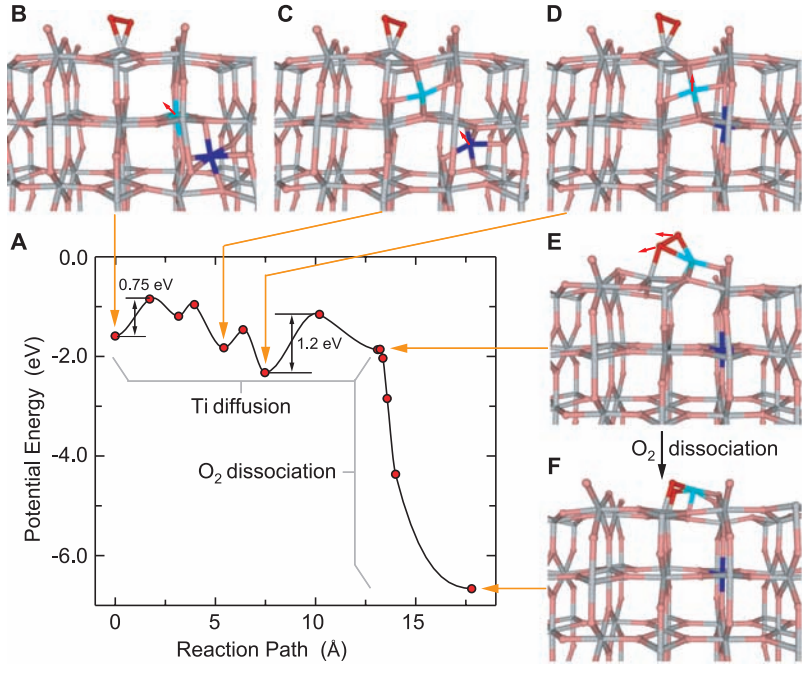

Fig. 5. (**A**) Potential-energy profile for the reaction of an adsorbed O_2 molecule and a Ti interstitial on TiO_2(110). The energy zero corresponds to O_2 in the gas phase and the Ti interstitial at the octahedral position between the second and third TiO_2 trilayer. (**B**) Adsorbed O_2 molecule (red). (**C**) Ti interstitial (dark blue) moved to tetrahedral position and lattice Ti (light blue) to tetrahedral position between the first and the second TiO_2 trilayer. (**D**) Original Ti interstitial (dark blue) now at lattice position. (**E**) Exchanged Ti interstitial (light blue) appearing at the surface. (**F**) Adsorbed O_2 dissociated and a surface TiO_2 island formed at the terrace. Orange arrows indicate positions on the potential-energy profile that correspond to the configurations shown in (B) to (F).

pared with a pair of nearest-neighbor O_{ot} adatoms (fig. S5C).

The role of the Ti interstitials in the O_2 adsorption and dissociation reactions is to provide the electronic charge for the adsorbates. According to the above Bader charge analysis, more electronic charge is required for dissociative adsorption ($2O_{ot}$) than for molecular adsorption ($1O_2$). Hence, dissociative adsorption is more sensitive to the amount of charge available on the surface than molecular adsorption, a fact clearly borne out by the DFT calculations in figs. S4 and S5. For instance, coadsorption of O_{ot} in fig. S5, B to D, decreases the stability of molecularly adsorbed O_2 by ~0.4 eV (fig. S5, B versus E) but that of dissociatively adsorbed oxygen by ~1.5 eV (fig. S5, C and D versus F and G). The coadsorbed O_{ot} adatom partially oxidizes the surface and thereby lowers the ease with which electronic charge is available for further surface reactions.

Within the scheme used for the calculations, the O_2 dissociation energy barrier is increased from ~0.3 to ~0.8 eV (fig. S5A) upon introduction of the O_{ot} adatom. This result explains why the coverage of O_{ot} adatoms remains low even under conditions in which the second O_2 dissociation channel operates (Fig. 3C); that is, the reaction is self-limiting. Similarly, some O_{br} vacancies remain unfilled even in the case of O_2 saturation (Figs. 1C and 4D); that is, the electronic charge required for the resulting O_{ot} adatoms depletes the source from the limited number of Ti interstitials. This charge-competition model also could explain why an O_2 desorption feature observed in the temperature-programmed desorption experiments by Henderson *et al*. (*30*) is evident only after exposing the *r*-TiO_2(110) surface at low temperature (below ~180 K). If impinging O_2 molecules can overcome the dissociation barrier, as observed in the experiments performed at RT (Fig. 3), the dissociation products deplete the electron donors in the bulk, and the accumulation of molecular O_2 is prohibited.

For a slab characterized by a Ti interstitial between the second and third TiO_2 trilayer and a pristine surface, our calculations reveal the existence of a gap state. This state lies ~2 eV above the VBM, in good agreement with the state observed in the PES experiments (Figs. 1D and 2E) as well as with DFT calculations addressing Ti interstitials in the bulk (*32*). A thorough analysis (fig. S6, A and B) of the spatially resolved electronic density of states shows that the gap state is spatially located in the region between the second and third TiO_2 trilayer, which strongly suggests that its origin is from the Ti interstitial. Further reduction of the surface layer by introduction of an O_{br} vacancy or a capping H atom (OH_{br} group) does not affect the gap state (fig. S6, C and D).

Conversely, adsorption of electronegative species such as O_2 or O_{ot} adatoms causes quenching of the gap state (fig. S6, E and F); in the case of adsorbed O_2, a new O_2-related state appears in the gap, in agreement with electron energy loss results by Henderson *et al*. (*30*). Most previous DFT papers addressing the gap state did not reveal a state in the gap for stoichiometric TiO_2 slabs with O_{br} vacancies or OH_{br} groups (*11*). Our calculations agree with these previous results (fig. S7, A to C) and further show no sign of a gap state when we introduce a hypothetical O vacancy in the bulk (fig. S7, D and E). These results challenge the conclusions derived by Di Valentin *et al*. (*10*) that a hybrid DFT setup is required to identify the gap state and that the gap state is related to O_{br} vacancies.

We propose that the surface redox chemistry on reduced titania is to a large extent associated with Ti interstitials in the near-surface region, because these defect sites provide the electronic charge, enabling important reactions. This conclusion is consistent with numerous experimental studies addressing the Ti*3d* defect state, including the pioneering work by Henrich *et al*. (*5*, *8*), electron paramagnetic resonance spectroscopy (*35*–*37*), bulk photonic (*38*) and transport (*39*) studies, recent photoelectron diffraction studies (*40*), and thin-film growth studies (*41*).

Moreover, several experimental results that were puzzling within an O vacancy model can now be revisited and explained more readily. For example, the simultaneous UPS and metastable impact electron spectroscopy (MIES) measurements of *r*-TiO_2(110) by Krischok *et al*. show no intensity between 0.5 to 1.0 eV below E_F in the MIES spectrum, whereas the Ti*3d* defect state is clearly observed in the UPS spectrum (*13*). Because of enhanced surface sensitivity with MIES as compared with UPS, the intensity of the Ti*3d* defect state is strongly suppressed in MIES (*13*). As a second example, it can be rationalized why the Ti*3d* defect state occurs for reduced bulk TiO_2 single crystals, but not for titania thin films grown on metal substrates. Particularly in the case of ultrathin titania films (*4*, *42*), there are no interstitial sites available and, hence, a defect state typical of reduced TiO_2 single crystals does not occur (*4*, *42*). Instead, the *d* electrons of the metal substrate can be considered a huge "bulk defect state" and thus fulfill the same function that the Ti interstitials do in reduced bulk TiO_2 crystals. Finally, at interfaces between two isolating oxide materials, the Ti interstitials may be the cornerstone to explain phenomena such as superconductivity, as has been reported for $LaAlO_3/SrTiO_3$ (*43*).

References and Notes

1. M. Haruta, T. Kobayashi, H. Sano, N. Yamada, *Chem. Lett.* **2**, 405 (1987).
2. M. Valden, X. Lai, D. W. Goodman, *Science* **281**, 1647 (1998).
3. D. Matthey *et al*., *Science* **315**, 1692 (2007).
4. M. Chen, Y. Cai, Z. Yan, D. W. Goodman, *J. Am. Chem. Soc.* **128**, 6341 (2006).
5. V. E. Henrich, P. Cox, *The Surface Science of Metal Oxides* (Cambridge Univ. Press, Cambridge, 1996).
6. U. Diebold, *Surf. Sci. Rep.* **48**, 53 (2003).
7. A. G. Thomas *et al*., *Phys. Rev. B* **75**, 035105 (2007).
8. V. E. Henrich, G. Dresselhaus, H. J. Zeiger, *Phys. Rev. Lett.* **36**, 1335 (1976).
9. T. L. Thompson, J. T. Yates, *Chem. Rev.* **106**, 4428 (2006).
10. C. Di Valentin, G. Pacchioni, A. Selloni, *Phys. Rev. Lett.* **97**, 166803 (2006).
11. M. V. Ganduglia-Pirovano, A. Hofmann, J. Sauer, *Surf. Sci. Rep.* **62**, 219 (2007).
12. R. L. Kurtz, R. Stockbauer, T. E. Madey, E. Roman, J. L. Desegovia, *Surf. Sci.* **218**, 178 (1989).
13. S. Krischok, J. Gűnster, D. W. Goodman, O. Höfft, V. Kempter, *Surf. Interface Anal.* **37**, 77 (2005).
14. S. Wendt *et al*., *Surf. Sci.* **598**, 226 (2005).
15. S. Wendt *et al*., *Phys. Rev. Lett.* **96**, 066107 (2006).
16. O. Bikondoa *et al*., *Nat. Mater.* **5**, 189 (2006).
17. Z. Zhang, O. Bondarchuk, B. D. Kay, J. M. White, Z. Dohnálek, *J. Phys. Chem. B* **110**, 21840 (2006).
18. J. V. Lauritsen *et al*., *Nanotechnology* **17**, 3436 (2006).
19. M. A. Henderson, *Surf. Sci.* **419**, 174 (1999).
20. K. T. Park, M. Pan, V. Meunier, E. W. Plummer, *Phys. Rev. B* **75**, 245415 (2007).
21. H. Iddir, S. Ogut, P. Zapol, N. D. Browning, *Phys. Rev. B* **75**, 073203 (2007).
22. H. Onishi, Y. Iwasawa, *Phys. Rev. Lett.* **76**, 791 (1996).
23. M. Li *et al*., *Surf. Sci.* **437**, 173 (1999).
24. R. A. Bennett, P. Stone, N. J. Price, M. Bowker, *Phys. Rev. Lett.* **82**, 3831 (1999).
25. M. A. Henderson, J. M. White, H. Uetsuka, H. Onishi, *J. Am. Chem. Soc.* **125**, 14974 (2003).
26. Materials and methods are available as supporting material on *Science* Online.
27. J. C. Woicik *et al*., *Phys. Rev. Lett.* **89**, 077401 (2002).
28. M. A. Henderson, W. S. Epling, C. H. F. Peden, C. L. Perkins, *J. Phys. Chem. B* **107**, 534 (2003).
29. W. S. Epling, C. H. F. Peden, M. A. Henderson, U. Diebold, *Surf. Sci.* **412-413**, 333 (1998).
30. M. A. Henderson, W. S. Epling, C. L. Perkins, C. H. F. Peden, U. Diebold, *J. Phys. Chem. B* **103**, 5328 (1999).
31. L. M. Liu, B. McAllister, H. Q. Ye, P. Hu, *J. Am. Chem. Soc.* **128**, 4017 (2006).
32. E. Cho *et al*., *Phys. Rev. B* **73**, 193202 (2006).
33. M. D. Rasmussen, L. M. Molina, B. Hammer, *J. Chem. Phys.* **120**, 988 (2004).
34. Z. Dohnálek, J. Kim, O. Bondarchuk, J. M. White, B. D. Kay, *J. Phys. Chem. B* **110**, 6229 (2006).
35. M. Li *et al*., *J. Phys. Chem. B* **104**, 4944 (2000).
36. A. L. Attwood, D. M. Murphy, J. L. Edwards, T. A. Egerton, R. W. Harrison, *Res. Chem. Intermediat.* **29**, 449 (2003).
37. M. Aono, R. R. Hasiguti, *Phys. Rev. B* **48**, 12406 (1993).
38. A. K. Ghosh, F. G. Wakim, R. R. Addiss, *Phys. Rev.* **184**, 979 (1969).
39. E. Yagi, R. R. Hasiguti, M. Aono, *Phys. Rev. B* **54**, 7945 (1996).
40. P. Krűger *et al*., *Phys. Rev. Lett.* **100**, 055501 (2008).
41. S. A. Chambers *et al*., *Chem. Phys.* **339**, 27 (2007).
42. P. Finetti *et al*., *J. Phys. Chem. C* **111**, 869 (2007).
43. N. Reyren *et al*., *Science* **317**, 1196 (2007).

44. We acknowledge financial support from the Danish Ministry of Science, Technology, and Innovation through iNANO, the Danish Research Councils, and the Danish Center for Scientific Computing. P.T.S. acknowledges support through NSF grants DMR-0504654 and CHE-0615606.

Supporting Online Material

www.sciencemag.org/cgi/content/full/1159846/DC1
Materials and Methods
Figs. S1 to S7
References

22 February 2008; accepted 28 May 2008
Published online 5 June 2008;
10.1126/science.1159846
Include this information when citing this paper.

The Role of Interstitial Sites in the Ti*3d* Defect State in the Band Gap of Titania

Stefan Wendt, Phillip T. Sprunger, Estephania Lira, Georg K. H. Madsen, Zheshen Li, Jonas Ø. Hansen, Jesper Matthiesen, Asger Blekinge-Rasmussen, Erik Lægsgaard, Bjørk Hammer and Flemming Besenbacher (June 5, 2008)

Science **320** (5884), 1755-1759. [doi: 10.1126/science.1159846] originally published online June 5, 2008

Editor's Summary

Science (print ISSN 0036-8075; online ISSN 1095-9203) is published weekly, except the last week in December, by the American Association for the Advancement of Science, 1200 New York Avenue NW, Washington, DC 20005.